Strongly coupled large-angle stimulated Raman scattering of short laser pulse in plasma-filled capillary

Serguei Kalmykov[a)]
Centre de Physique Théorique (UMR 7644 du CNRS), Ecole Polytechnique, 91128 Palaiseau cedex, France and Max-Planck-Institut für Quantenoptik, D-85748 Garching, Germany

Patrick Mora
Centre de Physique Théorique (UMR 7644 du CNRS), Ecole Polytechnique, 91128 Palaiseau cedex, France

(Received 2 April 2004; accepted 5 January 2005; published online 7 April 2005)

Strongly coupled large-angle stimulated Raman scattering (LA SRS) of a short intense laser pulse develops in a plane plasma-filled capillary differently than in a plasma with open boundaries. Coupling the laser pulse to a capillary seeds the LA SRS in the forward direction (scattering angle smaller than $\pi/2$) and can thus produce a high instability level in the vicinity of the entrance plane. In addition, oblique mirror reflections off capillary walls partly suppress the lateral convection of scattered radiation and increase the growth rate of the SRS under arbitrary (not too small) angle. Hence, the saturated convective gain falls with an angle much slower than in an unbounded plasma and even for the near-forward SRS can be close to that of the direct backscatter. At a large distance, the LA SRS evolution in the interior of the capillary is dominated by quasi-one-dimensional leaky modes whose damping is related to the leakage of scattered radiation through the walls. © *2005 American Institute of Physics*. [DOI: 10.1063/1.1862628]

I. INTRODUCTION

The technique of chirped-pulse amplification[1] made subpicosecond laser pulses of high power ($P>10^{12}$ W) available for generation of coherent x-rays,[2] high harmonics of radiation,[3] and laser wakefield acceleration (LWFA) of electrons[4–6] in rarefied plasmas [where $\omega_0 \gg \omega_{pe}$, ω_0 is a laser frequency, $\omega_{pe}=(4\pi e^2 n_0/m_e)^{1/2}$ is an electron plasma frequency, n_0 is a background electron density, m_e and $-|e|$ are the electron mass at rest and charge]. Full potential of these applications can be realized with the laser-plasma interaction length increased beyond the Rayleigh diffraction length, $z_R=\pi\sigma_0^2/\lambda_0$, by means of external optical guiding[6] (here and later, $\lambda_0 \approx 2\pi c/\omega_0$ is a laser wavelength and σ_0 is a laser beam waist radius). One of the guiding options is using a dielectric capillary,[7–9] where the oblique mirror reflections suppress the laser beam diffraction. Inside a capillary, plasma can be created by an optical field ionization of the filling gas[10–12] or by a laser ablation of the walls.[13] Then, the large-angle stimulated Raman scattering (LA SRS) starts to challenge transportation of a laser beam over a long distance.[14,15]

In the standard SRS process,[16] the pump electromagnetic wave (EMW) is scattered off spontaneous fluctuations of electron density, which, in turn, can be amplified by the ponderomotive beat wave of pump and scattered light. Appropriate phase matching of the waves results in a positive feedback loop with the onset of a spatiotemporal instability.[17] When the plasma extent is much larger than a laser pulse length and no reflections off plasma boundaries occur, both scattering electron plasma waves (EPW) and scattered EMW quit the region of amplification, and the convective gain saturates within a time interval of the order of pulse duration.[18–21] Given the pulse length, the maximum possible gain remains the same for *all* scattering angles, and whether it is achieved or not for a given angle is determined by the laser pulse aspect ratio only.[18–21] Convection of scattered radiation out of the laser waist may result in a strong pulse depletion.[22] Even when the full depletion does not occur, the LA SRS can produce considerable pulse erosion,[23] suppression of the relativistic self-focusing,[24] heating and preacceleration of plasma electrons,[25] and seeding the forward SRS.[26,27] Thereby, knowing the details of the LA SRS evolution in various physical conditions is a matter of high importance for applications.

Confining plasma by reflecting surfaces deeply modifies the SRS process. In the one-dimensional (1D) geometry, the Raman backscatter changes its nature from convective to absolute:[28] reflections trap the unstable radiation modes inside plasma and give rise to the continuous amplification. When the laser beam is confined between the mirror-reflecting partly transparent walls and propagates collinearly to them, reflections reduce the sideward convection of scattered light. If the reflective modes dominate in plasma, the LA SRS gain tends to that of the direct backscatter and thus reveals a dramatic increase in comparison with the open-boundary system.[14] The LA SRS in this geometry has been considered so far in the regime of weak coupling,[14] when the scattering EPW is similar to the plasma natural mode[17] and temporal growth rate is well below the electron plasma frequency. This regime requires fairly low amplitude of a laser pulse, i.e., $a_0 \ll \sqrt{\omega_{pe}/\omega_0} \ll 1$ [$a_0=eE_0/(m_e\omega_0 c)$ is a normalized amplitude of the laser electric field]. However, for the efficient LWFA,[4–6] the plasma density has to be reduced in order to increase the γ factor of the laser wakefield, $\gamma_g=\omega_0/\omega_{pe}$, and, hence, the electron energy gain. With $1/\gamma_g$

[a)]Present address: Department of Physics and Institute for Fusion Studies, The University of Texas at Austin, Austin, Texas 78712. Electronic mail: kalmykov@physics.utexas.edu

$<a_0^2<1$, the LA SRS becomes strongly coupled: its temporal growth rate exceeds ω_{pe} and the scattering EPW differs from the natural mode of plasma oscillations.[18,21,26,29,30] In a plasma-filled capillary, the strongly coupled LA SRS acquires new specific features: in a wide range of parameters relevant to the self-modulated LWFA,[5] our particle-in-cell (PIC) simulations [using the code WAKE (Ref. 31)] discovered a vast enhancement of the near-forward SRS in the immediate vicinity of the capillary entrance aperture. The unstable plasma modes were primarily transverse and therefore useless for the longitudinal electron acceleration. For the same range of parameters, this effect has never been significant in an open-boundary plasma. Independent fluid modeling[32] verified these observations.

Making a step to understanding this phenomenon we propose a two-dimensional (2D) linear theory of strongly coupled SRS of a short laser pulse under a given angle α in a slab of rarefied plasma laterally confined between the mirror-reflecting partly transparent flat walls (flat capillary). Boundary conditions for the scattered radiation describe the oblique mirror reflections and the electromagnetic (EM) seed at the entrance plane. We associate the latter with the signal formed of the high-order capillary eigenmodes produced by the laser beam coupling to the capillary (the coupling process is described elsewhere[8,11] and outlined in Appendix A). The forward ($\alpha<\pi/2$) and backward ($\alpha>\pi/2$) SRS proceed differently. Forward Raman amplification of the EM seed can be dominant within a finite distance from the entrance plane and be responsible for the instability enhancement observed in the modeling. On the other hand, the backward SRS is affected by the reflections only. As the LA SRS of a finite-length laser pulse preserves the convective nature (backward and, partly, sideward convection of radiation is allowed), the gain saturation occurs within a finite distance from the entrance plane. Reflections give the unstable modes additional rise time in any transverse cross section of a plasma, and, even for relatively small scattering angles (such as $\alpha=\pi/6$ taken for numerical examples of this paper), the saturated convective gain can approach that of the backward SRS (BSRS). The field structure is then approximated by a quasi-1D lossy mode whose damping is produced by the leakage of radiation through the walls.

The paper is organized as follows. Section II presents a theoretical model for the strongly coupled LA SRS in a 2D slab geometry. The laser pulse entrance into a plasma and oblique mirror reflections of scattered light are expressed in terms of appropriate boundary-value conditions for the coupled-mode equations. General solution of the boundary-value problem is presented (derivation is given in Appendix B). Section III discusses the spatiotemporal evolution of instability. The case of fully transparent lateral boundaries is considered in Sec. III A. Enhancement of the LA SRS in the generic reflective case is considered, and the maximum gain factors are evaluated in terms of appropriate asymptotic solutions in Sec. III B. Section IV summarizes the results.

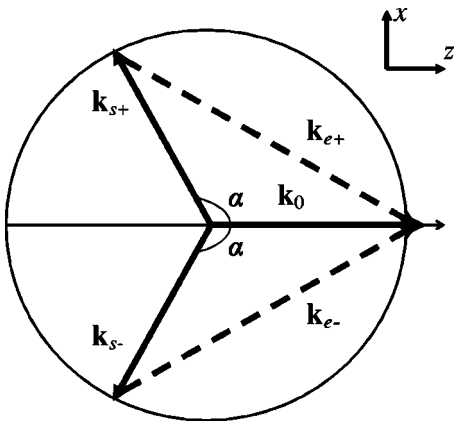

FIG. 1. Wave vector diagram of the LA SRS, "+" ("−") stands for the up-(down-)going interaction.

II. BASIC EQUATIONS AND SOLUTION OF BOUNDARY-VALUE PROBLEM

In a 2D plasma slab between the mirror-reflecting walls, the high-frequency (hf) electric field of the laser pulse and up- and down-going scattered EMW form a superposition

$$\mathbf{a}(\mathbf{r},t)=\frac{e^{-i\omega_0 t}}{2}\left\{\mathbf{a}_0(\mathbf{r},t)e^{ik_0 z}+\sum_{\sigma=\pm}\mathbf{a}_{s\sigma}(\mathbf{r},t)e^{i(\mathbf{k}_{s\sigma},\mathbf{r})}\right\}+\mathrm{c.c.}, \tag{1}$$

where $\mathbf{r}=(x,z)$ is a radius vector in a plane geometry. The normalized amplitudes $\mathbf{a}_0$ and $\mathbf{a}_{s\pm}=e\mathbf{E}_{s\pm}/(m_e\omega_0 c)$ ($|\mathbf{a}_{s\pm}|\ll|\mathbf{a}_0|<1$) refer to the linearly polarized electric field of pump and scattered radiation. The polarization vector $\mathbf{e}_p$ and laser wave vector $\mathbf{k}_0=\mathbf{e}_z k_0$ are parallel to the slab boundaries, and scattering under an angle α occurs in the plane orthogonal to $\mathbf{e}_p$. In the rarefied plasma, both $\mathbf{k}_0$ and $\mathbf{k}_{s\pm}$ obey the same dispersion relation $\omega_0^2=\omega_{\mathrm{pe}}^2+c^2k_{0(s\pm)}^2\approx c^2k_{0(s\pm)}^2$, hence, $|\mathbf{k}_{s\pm}|\equiv k_s=k_0$, $k_{s\pm z}\equiv k_{sz}=k_0\cos\alpha$, $\pm k_{s\pm x}\equiv k_{sx}=k_0\sin\alpha$, and the amplitudes $a_{0(s\pm)}$ vary slowly in time and space on the scales ω_0^{-1}, k_{sz}^{-1}, and k_{sx}^{-1}. Ions form a homogeneous positive background; this assumption holds for a laser pulse shorter than an ion plasma period, $t_0\ll 2\pi\omega_{\mathrm{pi}}^{-1}$. The beat wave of incident and scattered radiation excites perturbations of electron density,

$$\frac{n_e-n_0}{n_0}=\sum_{\sigma=\pm}N_\sigma^*(\mathbf{r},t)e^{i(\mathbf{k}_{e\sigma},\mathbf{r})}+\mathrm{c.c.}, \tag{2}$$

whose wave vectors obey the matching conditions $\mathbf{k}_{e\pm}=\mathbf{k}_0-\mathbf{k}_{s\pm}$; hence, $|\mathbf{k}_{e\pm}|\equiv k_e=2k_0\sin(\alpha/2)$, $k_{e\pm z}\equiv k_{ez}=k_0(1-\cos\alpha)$, $k_{e\pm x}=\mp k_0\sin\alpha$. Wave vector diagram of the LA SRS is shown in Fig. 1. The longitudinal component of phase velocity of the scattering EPW is small if compared with the speed of light, i.e., $k_{ez}>k_p\equiv\omega_{\mathrm{pe}}/c$. This restriction eliminates the near-forward Raman scattering[26,33] and resonant modulational instability (RMI).[34] In the rarefied plasma, the amplitudes $N_\pm$ vary slowly in space on the scales k_{ez}^{-1}, k_{ex}^{-1}.

The amplitudes of up- and down-going scattered EMW and scattering EPW obey the coupled-mode equations de-

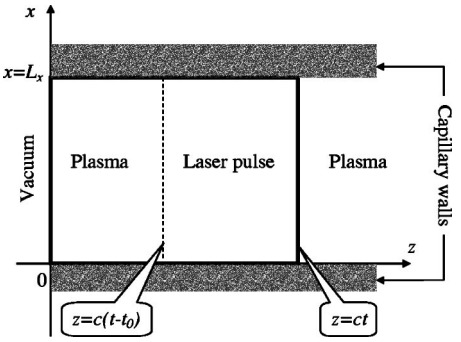

FIG. 2. Geometry of a laser pulse propagation in a laterally confined plasma. Laser pulse enters plasma at $z=0$ and $t=0$, and moves towards positive z. Boundary conditions are posed at the plasma boundary $z=0$, the pulse leading front $z=ct$, and the walls $x=0$ and $x=L_x$. Rear edge of the pulse $z=c(t-t_0)$ is a free boundary through which the waves quit the region of amplification. The boundary-value problem is solved in the area $c(t-t_0)<z<ct$, $0<x<L_x$.

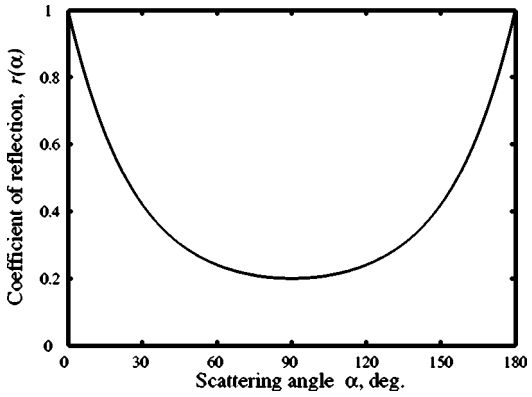

FIG. 3. Coefficient of reflection vs scattering angle for a glass wall with an index of refraction $\delta_w=1.5$ (the refraction index of plasma is taken equal to unity).

rived from the equations of nonrelativistic hydrodynamics of cold electron fluid in the hf field (1) and the Maxwell equations for scattered radiation,

$$i\left(\frac{\partial}{\partial\xi}+V_z\frac{\partial}{\partial z}\pm V_x\frac{\partial}{\partial x}\right)a_{s\pm}=g_1N_\pm, \tag{3a}$$

$$-\left(\frac{\partial^2}{\partial\xi^2}+k_p^2\right)N_\pm=g_2a_{s\pm}, \tag{3b}$$

where $V_z=\cos\alpha/(1-\cos\alpha)$, $V_x=\sin\alpha/(1-\cos\alpha)$, $g_1=(a_0/2)(k_p^2/k_{ez})$, and $g_2=a_0^*(k_e/2)^2$. The wave coupling parameter is $G^3\equiv g_1g_2=(a_0/2)^2k_p^2k_0$ (strong coupling is the case for $G\gg k_p$). Equations (3) are expressed through the variables x, z, and $\xi=ct-z$, that is, the temporal evolution of waves is traced in an x-y cross section at a longitudinal position z.

Figure 2 shows the interaction area. At $z=0$, $t=0$, the laser pulse enters a semi-infinite plasma-filled gap between flat mirror-reflecting walls $z\geqslant 0$, $0\leqslant x\leqslant L_x$ and propagates towards positive z. The pulse leading front, $\xi=0$, encounters the stationary level of electron density perturbations with a constant amplitude N_0,

$$N_\pm(x,z,0)=N_0, \tag{4a}$$

$$\partial N_\pm/\partial\xi(x,z,0)=0, \tag{4b}$$

fluctuations of radiation in fresh plasma being neglected,

$$a_{s\pm}(x,z,0)\equiv 0. \tag{5}$$

At the capillary entrance plane, the transverse profile of radiation can have a significant content of the high-order capillary eigenmodes (coupling the incident laser beam to the capillary is discussed elsewhere[8,11] and is outlined in Appendix A). The resonant condition for the wave vectors selects the modes that can be amplified by the forward SRS ($\alpha<\pi/2$) thus leading to the formation of an EM seed signal. To facilitate the forthcoming analytic job, we give this signal in a simple parabolic form with an amplitude vanishing at the walls in order to provide the continuity of the solution in the interior of the capillary,

$$a_{s\pm}(x,z=-0,\xi)=a_{s0}[1-(1-2x/L_x)^2]. \tag{6}$$

Inside the capillary, oblique mirror reflections couple up- and down-going EMW: each reflection converts an up-going wave into a down-going one and vice versa,

$$a_{s+}(0,z,\xi)=r(\alpha)a_{s-}(0,z,\xi), \tag{7a}$$

$$a_{s-}(L_x,z,\xi)=r(\alpha)a_{s+}(L_x,z,\xi). \tag{7b}$$

The conditions (7) set up a quasi-1D exponential behavior of waves at large z. The reflectivity coefficient is a known function of scattering angle, $r(\alpha)=|\sin\alpha-[(\delta_w/\delta_{\rm pl})^2-\cos^2\alpha]^{1/2}|/\{\sin\alpha+[(\delta_w/\delta_{\rm pl})^2-\cos^2\alpha]^{1/2}\}$, where δ_w and $\delta_{\rm pl}$ are the refraction indexes of walls and plasma. Figure 3 shows $r(\alpha)$ for a glass capillary with $\delta_w\approx 1.5$ and $\delta_{\rm pl}\approx 1$.

The temporal increment of strongly coupled LA SRS exceeds the electron plasma frequency. Hence, we neglect $k_p^2N_\pm$ in comparison with $\partial^2N_\pm/\partial\xi^2$ in the left-hand side (LHS) of Eq. (3b). With the allowance for not very tight capillary, the pump field envelope $a_0(x,\xi)$ represents a portion of laser radiation coupled to the capillary which experiences mostly paraxial propagation, $k_\perp/k_0\ll\sqrt{\omega_{\rm pe}/\omega_0}$. Assuming that the pump field evolution at a given point (x,z) takes much longer than the SRS growth ($z_R/c\gg t_0$), and in order to enable the analytic progress, we approximate $a_0(x,\xi)$ with a fixed flat profile at any position z in a capillary of the width L_x, $a_0(x,\xi)=a_0H(x)H(L_x-x)H(\xi)H(ct_0-\xi)$, using the effective pulse duration t_0 and amplitude a_0. Here and below, $H(y)$ is the Heaviside step function. Solution of the boundary-value problem,

$$a_{s+}(\mathbf{R};r)=\frac{g_1N_0}{3i}\sum_{j=1}^{3}\frac{e^{c_j\xi}}{c_j}[1-\Phi_{1D}(\mathbf{R};r,c_j)-\Phi_{2D}(\mathbf{R};r,c_j)]$$
$$-a_{s0}\sqrt{\pi}\mathcal{F}(\mathbf{R};r)_0\tilde{F}_2(;1,1/2;i\zeta) \tag{8a}$$

$$N_+(\mathbf{R};r) = \frac{N_0}{3}\sum_{j=1}^{3} e^{c_j\xi}[1-\Phi_{1D}(\mathbf{R};r,c_j)-\Phi_{2D}(\mathbf{R};r,c_j)] + a_{s0}(\sqrt{\pi}/4)g_2\mathcal{F}(\mathbf{R};r)\left(\xi - z/V_z\right)^2 {}_0\tilde{F}_2\left(;2,3/2;i\zeta\right) \tag{8b}$$

is then obtained via the 2D Laplace transform; here, $\mathbf{R}=(\mathbf{r},\xi)$, $c_j^3=iG^3$, $\zeta=(G^3/4)(\xi-z/V_z)^2 z/V_z$, ${}_0\tilde{F}_2(;b_1,b_2;i\zeta)$ is the regularized generalized hypergeometric function,[35]

$$\Phi_{1D} = F_s\left(c_j,\frac{z}{V_z},\xi\right)\left\{H(V_z x - V_x z) + \sum_{n=1}^{\infty} r^n \times[H(V_x z - V_z x_{n-1}) - H(V_x z - V_z x_n)]\right\}, \tag{9a}$$

$$\Phi_{2D} = (1-r)\sum_{n=0}^{\infty} r^n F_s\left(c_j,\frac{x_n}{V_x},\xi\right)H(V_x z - V_z x_n), \tag{9b}$$

$$\mathcal{F} = \left\{\frac{(V_z x - V_x z)(V_z x - V_x z - V_z L_x)}{(V_z L_x/2)^2}H(V_z x - V_x z) + \sum_{n=1}^{\infty} r^n \frac{(V_z x_{n-1} - V_x z)(V_z x_n - V_x z)}{(V_z L_x/2)^2}[H(V_x z - V_z x_{n-1}) - H(V_x z - V_z x_n)]\right\} H\left(\xi - \frac{z}{V_z}\right), \tag{9c}$$

where $x_n = x + nL_x$ and the fundamental solution $F_s(\mu,\nu,\xi)$ (Ref. 21) is defined by Eq. (B6). The up- and down-going amplitudes are symmetric, $a_{s-}(x)=a_{s+}(L_x-x)$, $N_-(x)=N_+(L_x-x)$, so we consider below the evolution up-going waves only. Our solution possesses the same generic structure as the weakly coupled reflective solution discussed in detail in Ref. 14. However, contrary to the case of semi-infinite laser pulse of Ref. 14, the growth time of unstable waves is now limited by the pulse duration t_0, and, as shown in Sec. III B, the gain at a given point (x,z) remains finite and is given by either Eq. (15) or Eq. (16).

III. SPATIO-TEMPORAL EVOLUTION OF UNSTABLE WAVES

A. Evolution of instability in open-boundary system

When the lateral boundaries are fully transparent, $r=0$, the EM seed at the entrance plane vanishes ($a_{s0}=0$), and the instability grows from the electron density noise in a fresh plasma ahead of the pulse. The functions (9) then read

$$\Phi_{1D}(\mathbf{R};r,c_j) = F_s(c_j, z/V_z, \xi)H(V_z x - V_x z),$$

$$\Phi_{2D}(\mathbf{R};r,c_j) = F_s(c_j, x/V_x, \xi)H(V_x z - V_z x).$$

Plasma is divided by the characteristics $\xi=z/V_z$, $x=z(V_x/V_z)$, $\xi=x/V_x$, into ranges of dependence, where the solution is prescribed by the boundary conditions for radiation posed at the pulse leading edge $\xi=0$ (range I),

$$\left.\begin{array}{l}\xi < x/V_x\\ \xi < z/V_z\end{array}\right\} \Rightarrow \Phi_{1D}\equiv 0, \quad \Phi_{2D}\equiv 0 \tag{10}$$

at the wall $x=0$ (range II),

$$\left.\begin{array}{l}x < z(V_x/V_z)\\ \xi > x/V_x\end{array}\right\} \Rightarrow \Phi_{1D}\equiv 0, \quad \Phi_{2D}\not\equiv 0 \tag{11}$$

or at the entrance plane $z=-0$ (range III),

$$\left.\begin{array}{l}x > z(V_x/V_z)\\ \xi > z/V_z\end{array}\right\} \Rightarrow \Phi_{1D}\not\equiv 0, \quad \Phi_{2D}\equiv 0. \tag{12}$$

The principal feature that makes the LA SRS of a short pulse[21] different from the case of semi-infinite laser beam[19] is the gain saturation within a finite distance from the entrance plane. At some point, $z_{sat}<+\infty$, the scattered radiation arriving from the plasma boundary $z=-0$ drops behind the laser pulse, and in all the points $z>z_{sat}$ neither part of the pulse belongs to the range III. Then, the evolution of waves and the gain do not alter with z. The gain saturates differently for the "forward" ($\alpha<\pi/2$) and "backward" ($\alpha>\pi/2$) scattering.

When $\alpha<\pi/2$, and the distance from the entrance plane is not too large, i.e., $z<\min\{V_z ct_0, L_x(V_z/V_x)\}$, all three areas (10)–(12) are available in the pulse body (that is, within a rectangle $0\leqslant\xi\leqslant ct_0$, $0\leqslant x\leqslant L_x$). Given the point (x,z), waves fall initially within a range I, where they grow in time exponentially with an angle-independent increment

$$\gamma_0 = (\sqrt{3}c/2)G \approx (\sqrt{3}/2)\sqrt[3]{(a_0/2)^2\omega_0\omega_{pe}^2}. \tag{13}$$

Note that $\kappa=\gamma_0/c$ is the known "spatial" increment of the strongly coupled BSRS in the comoving frame.[6,18,20,21,26,30] The evolution of waves is strictly 1D in space on this stage. Later, information from the boundaries $x=0$ and $z=-0$ reaches the point (x,z), and the spatial dependence becomes either 2D for $\xi>x/V_x$, $x<z(V_x/V_z)$ (range II) or remains 1D for $\xi>z/V_z$, $x>z(V_x/V_z)$ (range III). The waves are not exponentially growing at this time. In the range III, the entrance effect dominates: vanishing the scattered EMW at the boundary $z=-0$ determines the behavior of 1D amplitudes. Deeply enough in plasma, $z\geqslant\min\{V_z ct_0, L_x(V_z/V_x)\}$, the entrance effect vanishes as the pulse terminates sooner than the scattered EMW from the entrance plane can reach the observer at given z. The pulse body is then divided between the ranges I and II, and the evolution of LA SRS is the same through the rest of the plasma.

For $\alpha>\pi/2$, the boundary-value condition posed for radiation at $z=-0$ can only produce the scattered EMW convecting outwards (the EMW characteristic $\xi=z/V_z$ recasts in the lab frame variables as $z=-ct|\cos\alpha|$ and corresponds to the wave propagating towards negative z). Thus, the entrance effect does not change the solution at a positive z, and the boundary-value condition (6) becomes excessive (this is also valid in the reflective case). The spatiotemporal evolution of the LA SRS remains the same at any $z\geqslant 0$.

Given the pulse duration, the maximum of the saturated gain, a_{s+}, $N_+\sim e^{\gamma_0 t_0}$, does not depend on the scattering angle, and whether it is achieved or not is determined solely by the pulse aspect ratio.[21] If the pulse is wide, or the scattering

angle is sufficiently large, $\alpha > \alpha_0 = 2\arctan(ct_0/L_x)$, the maximum gain is achieved at the pulse rear edge $\xi = ct_0$ for $ct_0\cot(\alpha/2) < x < L_x$. Hence, the angular spectrum of scattered light is prescribed by the pulse aspect ratio rather than the angular dependence of the increment. For $L_x \gg ct_0$, scattering within a broad range of angles $2ct_0/L_x < \alpha \leqslant \pi$ proceeds with the maximum gain. Otherwise, for $L_x \ll ct_0$, the highest gain corresponds to the near-backward scattering only, $\pi - L_x/(ct_0) < \alpha \leqslant \pi$ (Ref. 21). To estimate the pulse energy depletion due to the LA SRS, it is sufficient to neglect the radiation scattered under angles smaller than α_0 (Ref. 36).

B. LA SRS evolution in the reflective case

In a capillary, the oblique mirror reflections of scattered light off the walls [the boundary condition (7)] contribute to the LA SRS evolution over the whole laser path in plasma, but become actually dominating later, when the entrance effect vanishes ($z > V_z ct_0$). The reflections establish a long-distance asymptotic state of the LA SRS—amplification of a quasi-1D radiation and plasma modes with a temporal increment close to that of the direct backscatter (13). Besides, the forward SRS is seeded by the EM signal $a_{s+}(x,-0,\xi)$ at the capillary entrance plane [the boundary condition (6)]. If the signal amplitude a_{s0} exceeds the amplitude of the electron density noise N_0, the unstable waves will achieve a large amplitude (by virtue of the high seed level) at the transient stage of laser propagation, $0 < z < V_z ct_0$. In this case, contrary to the SRS in the unbounded plasmas described in the preceding section, the near-forward SRS exhibits a much higher level of amplification than the backward SRS ($\alpha > \pi/2$), and its contribution to the dynamics of electron density perturbations can be dominating. Nonlinearities of plasma response that can then appear are worth investigating and will be addressed in future publications.

The asymptotic ${}_0\tilde{F}_2(;b_1,b_2;i\zeta) \sim (2\pi\sqrt{3})^{-1}(i\zeta)^{(1-b_1-b_2)/3} \times e^{3\sqrt[3]{i\zeta}} + O(1/\sqrt[3]{i\zeta})$ at $|\zeta| \to \infty$ (Ref. 35) helps to evaluate the level of the EM seed amplification on the interval $0 < z < V_z ct_0$,

$$|a_{s+}(z < V_z ct_0)| \sim a_{s0} \frac{\mathcal{F}}{2\sqrt{3\pi}} \frac{e^{3\sqrt{3}\zeta^{1/3}/2}}{\zeta^{1/6}}, \tag{14}$$

where $\zeta \gg 1$. Then, $|N_+(z < V_z ct_0)| \sim (V_z/g_1)(\zeta^{1/3}/z)|a_{s+}|$. At the pulse trailing edge, $\xi_0 = ct_0$, the argument of the asymptotic reaches the maximum $\zeta_{\max} = (Gct_0/3)^3$ at $z_{\max} = V_z ct_0/3$. At this point, the scattered EPW reaches the amplitude

$$|N_+(\xi_0, z_{\max})| \sim a_{s0} \frac{G}{g_1} \frac{\sqrt[4]{3}\mathcal{F}}{\sqrt{8\pi}} \frac{e^{\gamma_0 t_0}}{\sqrt{\gamma_0 t_0}}, \tag{15}$$

and $|a_{s+}(\xi_0, z_{\max})| \sim (g_1/G)|N_+(\xi_0, z_{\max})|$. Equation (15) shows that the maximum gain on the transient stage is determined by the 1D temporal increment (13) independent on α (the angular dependence is retained in the preexponential factors only). For the minimally allowed scattering angle, $\alpha_{\min} = \sqrt{2\omega_{pe}/\omega_0}$ (hence, $V_z \approx \omega_0/\omega_{pe}$), the point of the maximal gain is $z_{\max}(\alpha_{\min}) \approx (\omega_0/\omega_{pe})(ct_0/3) \gg ct_0$. Parameters of the following numerical example (Fig. 4) give $z_{\max}(\alpha_{\min}) \approx 3$ mm, which is shorter than a typical capillary length used in experiments ($\geqslant 1$ cm).[8–13,15]

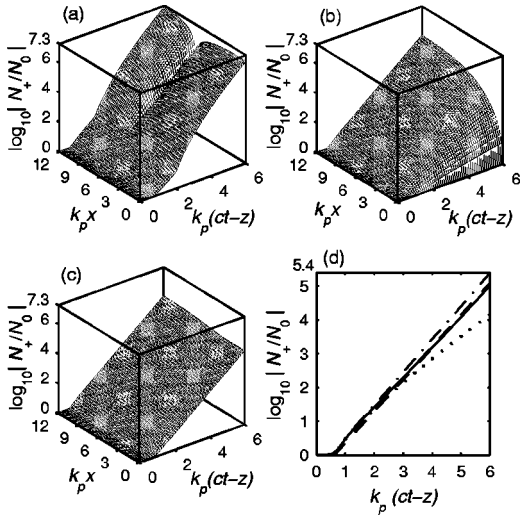

FIG. 4. Spatiotemporal evolution of the up-going EPW in the field of transversely limited laser pulse of finite duration; the pulse aspect ratio is $ct_0/L_x = 0.5$. The scattering angle is $\alpha = \pi/6$. Temporal evolution of the amplitudes is traced at the longitudinal positions (a) $z = V_z ct_0/3 \approx 2.2ct_0$, and (c), (d) $z = V_x ct_0 \approx 6.5ct_0$. The left column shows the SRS evolution inside the glass capillary ($r = 0.42$) with the EM seed amplitude at the entrance plane $a_{s0} = 0.4 \times 10^{-5}$. Plot (b) shows the saturated solution for an open-boundary plasma, $r = a_{s0} = 0$, for $z > (V_z/V_x)ct_0 \approx 3.4ct_0$. In the plot (d), the long-term asymptotic (16) of the reflective problem (dashed line) is compared with the exact solution (solid line) and with nonreflective (dotted line) and BSRS (dash-dotted line) solutions at the point $z = V_z ct_0$, $x = L_x/4$.

For $z > z_{\max}$ the entrance effect becomes less pronounced and finally vanishes at the point $z = V_z ct_0 = 3z_{\max}$, where the EM signal arriving from $z = -0$ drops behind the laser pulse and the instability growth saturates. Evolution of both forward and backward scattering is then determined by the lateral reflections only and, given the scattering angle, remains the same in any x-y cross section for $z \geqslant V_z ct_0$. We show in Appendix C that at $z \geqslant V_z ct_0$ and $\gamma_0 t_0 > 1$, a cumbersome exact solution (8) admits a simple asymptotic evaluation in the form of quasi-1D damped mode with a temporal growth rate close to (13),

$$N_+(x,\xi) \sim (N_0/3)[(1-r)/\ln r] e^{s_0 \xi - (x/L_x)\ln r}, \tag{16}$$

and $a_{s+}(x,\xi)$ is given by Eq. (C2). Here, $s_0 = (\gamma_0 - \Delta\gamma)/c$, $\Delta\gamma/c \approx -V_x \ln r/(3L_x)$. Equations (16) and (C2) are valid under the "low leakage" condition, $r > \exp(-3GL_x/V_x)$, which indicates that the scattered light is mostly trapped inside a plasma slab: the energy leakage through the wall at one reflection (that produces an effective decrement $\Delta\gamma \ll \gamma_0$) is less than the energy gain on the way between the walls. The lateral growth of the asymptotic (16) is much slower than the growth with ξ. Asymptotic solution (16) displays the basic result of the reflective theory of the LA SRS: at large distances from the entrance plane and large coefficients of amplification, the amplitudes of unstable waves tend to quasi-1D leaky modes exponentially growing in time with the increment tending to that of the BSRS (13).

Comparison of Eqs. (15) and (16) shows that the maximum amplitude of the scattering EPW on the transient stage, $z<V_z ct_0$, differs from the final asymptotic level of density perturbations roughly by a factor of $(G/g_1)\times(\gamma_0 t_0)^{-1/2}(a_{s0}/N_0)$. When this factor is larger than unity, and $|N_+(z\geqslant V_z ct_0, x, ct_0)|\sim 1$, the plasma response can become nonlinear in the vicinity of $z=V_z ct_0/3$. This could be avoided by keeping the ratio of the seed amplitudes a_{s0}/N_0 below $(g_1/G)(\gamma_0 t_0)^{1/2}$. The amplitude of the electron density noise is difficult to control in experiment; however, as shown in Appendix A, the content of the high-order eigenmodes in the laser radiation coupled to the capillary (and, hence, the amplitude a_{s0} of the EM seed signal) can be effectively reduced by increasing the capillary radius versus the radius of the incident laser beam.

Figure 4 shows the spatiotemporal evolution of an up-going EPW [Eq. (8b)] for the SRS under the angle $\alpha=\pi/6$. The laser and plasma parameters are $a_0=0.7$, $\lambda_0=0.5\ \mu$m, $ct_0=0.5L_x=6k_p^{-1}$, $\omega_{pe}/\omega_0=0.007$, which give $n_0\approx 2.2\times 10^{17}\ \mathrm{cm}^{-3}$, the pulse duration $t_0\approx 230$ fs, and the maximum increment $\gamma_0\approx 2.25\omega_{pe}$. The level of EM seed is chosen as $a_{s0}\approx 0.58\times 10^{-5}a_0$ (according to Appendix A, it corresponds to a capillary by a factor of 2 wider than in the case of perfect matching; by the definition, in axisymmetric geometry, the perfect matching condition provides coupling 98% of energy of an incident Gaussian laser pulse to the fundamental eigenmode EH_{11} of a capillary[8]). The level of the plasma noise evaluated in Appendix A is $N_0\approx 1.5\times 10^{-6}$. The plots (a) and (c) correspond to the plasma confined in a glass capillary with the reflection coefficient $r=0.42$ (see Fig. 3), and (b) corresponds to the unbound plasma ($r=0$ and $a_{s0}=0$); plot (d) shows the long-term asymptotic behavior of the reflective solution. The plasma cross sections are set at (a) $z=V_z ct_0/3\approx 2.2ct_0$, and (c), (d) $z=V_z ct_0\approx 6.5ct_0$. Given the calculation parameters, the nonreflective solution saturates at $z=L_x(V_z/V_x)\approx 3.4ct_0$ and is exactly the same in any plasma cross section x-y beyond that point. Figure 4(b) shows this solution. The ranges of influence of boundary conditions are shown in Fig. 5. In range I [see Eq. (10)], the electron density noise from $\xi=0$ is amplified and the waves do not experience reflections. In range IIa the instability is seeded by the free-plasma noise, and yet is enhanced by the reflections; the Raman amplified signal arriving from the entrance plane is added to these waves in range IIb The EM seed from the entrance plane $z=-0$ is amplified by the forward SRS in range III.

In a capillary, the forward SRS is considerably enhanced at $z<V_z ct_0$ (roughly by a factor of 70 in amplitude) versus the case of unbound plasma [compare Figs. 4(a) and 4(b)]. Despite the EM seed amplified in range IIb is nonexponentially growing, the high ratio of seed amplitudes, $a_{s0}/N_0\approx 2.7\geqslant(g_1/G)(\gamma_0 t_0)^{1/2}\approx 0.026$, makes the entrance effect rather pronounced [Fig. 4(a)]. For $N_0\approx 1.5\times 10^{-6}$ and $\mathcal{F}\sim 1$, Eq. (15) gives $\log_{10}|N_+(\xi_0, z_{max})/N_0|\approx 7.15$, which agrees with Fig. 4(a). Hence, parameters of the numerical example lay at the border of validity of the linear approach, and increase in a_{s0} will result in the nonlinearity of the plasma response on the transient stage [e.g., perfect matching gives $a_{0s}\approx 0.012a_0$, hence, according to Eq. (15),

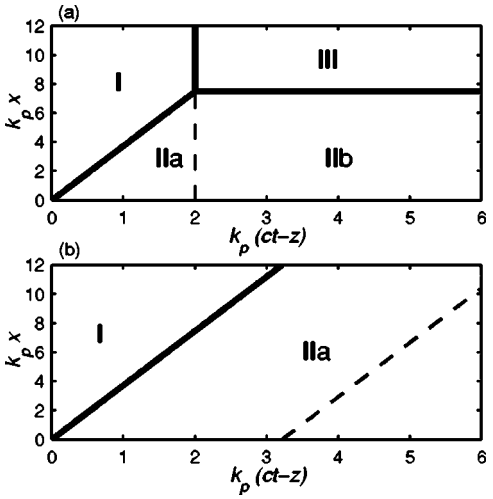

FIG. 5. Ranges of dependence for the SRS under the angle $\alpha=\pi/6$ in the cross sections at (a) $z=V_z ct_0/3\approx 2.2ct_0$ and (b) $z=V_x ct_0\approx 6.5ct_0$. The thick solid line $x=z(V_x/V_z)$ divides the principal ranges prescribed by the nonreflective theory. The dashed lines are the characteristics of reflected waves, $x+nL_x=z(V_x/V_z)$, $\xi=z/V_z$, and $\xi\ (x+nL_x)/V_x$. One reflection contributes to the scattering process in the range II in the case (a) and two reflections in the case (b). Raman amplification of the EM signal given at the boundary $z=-0$ contributes to the solution in the subrange IIb and range III.

$|N_+(\xi_0, z_{max})|\sim 10^6$; this burst of the forward SRS has been the regular feature in our numerical experiments and in the fluid simulations[32]. On the other hand, reducing a_{s0} to the level $7\times 10^{-8}a_0$ (which in the axisymmetric case would correspond to a capillary tube by a factor 2.5 wider than in the case of perfect matching, see Appendix A) will make the forward Raman amplification of the EM seed almost negligible and thus tolerable on the transient stage.

Figure 4(c) shows a quasi-1D saturated solution [compare with Fig. 4(b)] thus shaped by the contribution from two reflections [according to Fig. 5(b)], which, in full agreement with the long-scale asymptotic (16), demonstrates the growth rate close to that of BSRS. Difference between Figs. 4(a) and 4(c) shows that, under the parameters of our example, the forward scattering ($\alpha<\pi/2$) is characterized at $z<V_z ct_0$ by a much higher gain than the SRS in the backward direction ($\alpha>\pi/2$). This situation is completely reverse of the SRS in an unbounded plasma, where the gain can only fall as an angle drops.[18] So, the higher the EM seed level produced by the laser beam coupling (that is, the tighter the capillary in a numerical or real-scale experiment), the more important becomes the forward SRS. In such case, a high amplification level of waves may be observed within quite a long distance in plasma, $z<V_z(\alpha_{min})ct_0\approx(\omega_0/\omega_{pe})ct_0$ [see also the discussion following Eq. (15)]. This effect is adverse for such applications as the self-modulated LWFA in capillaries.[15] The way of reducing the excessive forward SRS enhancement can be found in using a wider capillary (the laser focal spot fixed) than the perfect matching requires.

Figure 4(d) traces the temporal evolution of the up-going EPW at $x=L_x/4$ (near the capillary wall). The asymptotic (16) perfectly approximates (and, for applications, can be used instead of) the exact reflective solution (8b). The dash-dotted and dotted lines in Fig. 4(d) correspond to the BSRS

solution $|N_+(\xi)| \approx (N_0/3)\exp(\gamma_0\xi/c)$ and the exact nonreflective solution, respectively, providing the upper and lower limits of the convective gain variation. In this example, only in the vicinity of the border $x=0$ the coefficients of amplification in the reflective and nonreflective cases are considerably different [compare Figs. 4(b) and 4(c)]. Contribution from the reflections increases the wave amplitude at $x=L_x/4$ by roughly an order of magnitude (compare solid and dotted lines at $k_p\xi \approx 6$). For the parameters chosen, the scattering EPW remains linear in the convective saturated regime ($z > V_z c t_0$): the plasma noise level, $N_0 \approx 1.5\times 10^{-6}$, substituted into Eq. (16), gives $|N_+| \leq 0.2$ throughout the whole time interval $0 < t < t_0$.

In the limit $r \to 1$ the total suppression of the lateral convection occurs. The up- and down-going amplitudes (8) become purely one dimensional for $z > V_z c t_0$ and completely identical. These amplitudes grow in time exponentially with the BSRS increment (13).

IV. CONCLUSION

We have proposed a 2D nonstationary linear theory of strongly coupled LA SRS of a short laser pulse in a flat plasma slab confined between mirror-reflecting walls (flat capillary). In a capillary, the lateral convection of scattered light is partly suppressed by the oblique reflections, and the instability experiences an enhancement. Additional enhancement of the SRS in forward direction ($\alpha > \pi/2$) is produced by the amplification of the electromagnetic seed signal that is formed of the high-order capillary eigenmodes at the entrance plane (formation of the signal is a consequence of the laser beam coupling to the capillary). The convective nature of LA SRS does not change. The asymptotic behavior of the waves demonstrates the transition from the set of 2D modes to the dominant quasi-1D damped mode. Even for near-forward scattering the convective gain of the dominant quasi-1D mode may be close to the BSRS gain.

ACKNOWLEDGMENTS

The authors wish to acknowledge useful conversations with N. E. Andreev, B. Cros, L. M. Gorbunov, G. Matthieussent, and J. Meyer-ter-Vehn. S.Y.K. sincerely appreciates hospitality of the Ecole Polytechnique and the Max-Planck-Institut für Quantenoptik and their financial support in the form of postdoctoral fellowships.

APPENDIX A: SEED SOURCES FOR LA SRS

The LA SRS under arbitrary angle in strongly rarefied plasmas ($\omega_{pe} \ll \omega_0$) is seeded by spontaneous electron density fluctuations ahead of the pulse. A root-mean-square (rms) amplitude of these fluctuations is represented in the equations by the quantity N_0, which gives the amount of seed corresponding to the element of solid angle $d\Omega_{\mathbf{k}_e}$ in the direction of the wave vector $\mathbf{k}_e$ of scattering EPW, and can be expressed as $N_0^2(k_e) = d\Omega_{k_e} \int n_e^{3D} k^2 dk \approx n_e^{3D}(k_e) k_e^2 \Delta k_e d\Omega_{\mathbf{k}_e}$, where $n_e^{3D}(k_e)$ is a spectral density of electron fluctuations integrated over frequencies.[37] The integral is taken over the area of maximal spectral density of scattering EPW [$k \approx k_e$, the amplification bandwidth $c\Delta k_e \approx 4\sqrt{\gamma_0/t_0}$ is estimated at $\gamma_0 t_0 \gg 1$ with taking account of the gain narrowing (Ref. 36)]. Using the ratio of the phase volumes $|d\mathbf{k}_e/d\mathbf{k}_s| = 2\sin^2(\alpha/2)$ (Ref. 38), we express the seed amplitude through the element of solid angle $d\Omega_{\mathbf{k}_s}$, in the direction of detector, $N_0^2 \approx (8/c) n_e^{3D}(k_e) k_0^2 \sqrt{\gamma_0/t_0} \sin^2(\alpha/2) d\Omega_{\mathbf{k}_s}$. Our theoretical formalism based on the assumption of quasiplane interacting waves requires small variation of the scattered wave amplitude across the direction $\mathbf{k}_s$ in the transversely limited area, $0 \leq x \leq L_x$, which gives an estimate of the angular spread $\Delta\alpha \approx \cos\alpha/(L_x k_0)$. The element of solid angle then evaluated as $\Delta\Omega_{\mathbf{k}_s} \approx 2\pi \sin\alpha \Delta\alpha = \pi \sin 2\alpha/(L_x k_0)$ gives

$$|N_0| \approx \left[\frac{8\pi}{n_0 \lambda_0^3} \frac{1 + (k_e r_{De})^2}{2 + (k_e r_{De})^2} \frac{(\gamma_0 t_0)^{1/2}}{(\omega_0 t_0)^{3/2}} \frac{\sin^2(\alpha/2)\sin 2\alpha}{k_0 L_x} \right]^{1/2}, \tag{A1}$$

where the spectral density of low-frequency electron fluctuations $n_e^{3D}(k_e)$ is evaluated using formula (11.2.6.6) of Ref. 37. Parameters of Fig. 4 and $k_e r_{De} \ll 1$ give $|N_0| \approx 1.5\times 10^{-6}$.

For the strongly coupled SRS in the forward direction ($\alpha < \pi/2$), coupling the laser beam to a capillary creates an additional source of instability. The radial profile of an incident beam with the wings cut off by the edges of the entrance aperture is approximated with an expansion through an infinite number of radial eigenmodes (having the same frequency ω_0).[7,8] The high-order eigenmodes (characterized by the frequency $\omega_s = \omega_0$ and high transverse wave numbers, $k_{n\perp} \sim k_{sx}$, where the integer n is the mode order) form the seed signal that is further amplified in plasma by the SRS [in the model form, the transverse profile of this signal is given by Eq. (6)]. It should be emphasized that these modes provide no seed for the weakly coupled SRS [including near-forward SRS and RMI (Ref. 34) that correspond to small scattering angles, $\alpha \ll \sqrt{\omega_{pe}/\omega_0}$], as this process requires the frequency matching $\omega_s \approx \omega_0 - \omega_{pe}$ between the seed and the pump.

Exact functional form of the capillary eigenmodes depends on the geometry chosen. Despite the LA SRS in a flat capillary is considered in the paper, we suppose that an estimate of the EM seed level will be more useful for applications if inferred from the axisymmetric theory of the laser beam propagation in a dielectric tube.[7,8] The theory represents an electric field profile at the entrance aperture of the radius r_0 as an infinite sum $\tilde{a}(r) = a_0 \Sigma_{n=1}^{+\infty} C_n J_0(k_{n\perp} r)$ (Ref. 11), where $C_n = 2[r_0 J_1(u_n)]^{-2} \int_0^{r_0} a(r) J_0(u_n r/r_0) r\, dr$ is the overlap integral of the hybrid capillary eigenmode EH_{1n} with the incident laser profile $a(r) = \exp(-r^2/\sigma_0^2)$ (Fig. 6). Here, u_n is the nth zero of the zero-order Bessel function of the first kind, $J_0(u_n) = 0$; for $k_0 r_0 \gg 1$ and $n \gg 1$, $k_{n\perp} r_0 \approx u_n \approx (n + 1/2)\pi$. Figure 6 shows that about 98% of laser energy is coupled to the fundamental mode for $\sigma_0 = 0.645 r_0$ (the perfect matching condition); however, the overlap integral decays very slowly as n grows {the analytic fit, $C_n \sim F_n = \exp[-(n+50)^{0.3}]$, is almost exact for $n > 10$}. When the ratio σ_0/r_0 drops, the larger number of lower-order eigenmodes is effectively excited (up to 5 for $\sigma_0 = 0.258 r_0$), but contribution from the higher-order modes into the radiation profile at $z = -0$ drops sharply (e.g., analytic fit $C_n \approx 3\times 10^{-6} F_n$, n

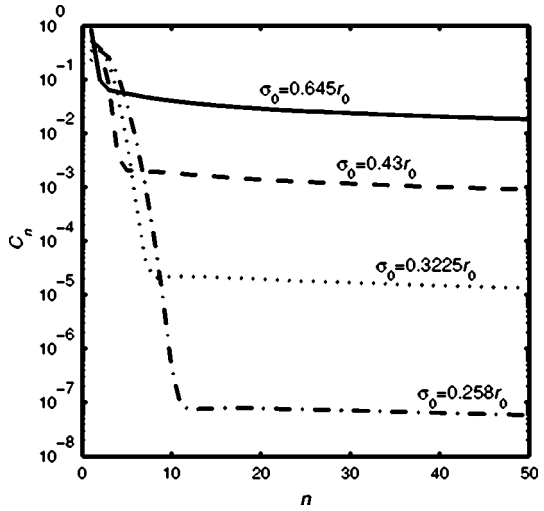

FIG. 6. Overlap integral between the radial profiles of amplitude of the incident laser (Gaussian) and of the capillary hybrid eigenmodes EH_{1n}.

>10, holds for $\sigma_0=0.258r_0$). Therefore, choosing wider capillary is the way of reducing the effect of laser coupling on the forward strongly coupled SRS.

The numerical example of Sec. III B shows how the SRS under the angle $\alpha=\pi/6$ develops in the capillary with an EM seed amplitude characteristic of the axisymmetric capillary tube by a factor of 2 wider than in the case of perfect matching. For the parameters of Fig. 4, with the value $L_x/2 \approx 860k_0^{-1}$ assigned to r_0, equalizing the effective radial wave number $k_{n\perp}\approx n\pi/r_0$ to the resonant wave number $k_{s\perp}=k_0\sin\alpha$ gives the resonant mode order $n^*\approx(k_0r_0/\pi)\sin\alpha \approx 136$ corresponding to $C_{136}\approx 0.58\times10^{-5}$ under the condition $\sigma_0=0.3225r_0$ (analytic fit $C_n\approx 0.7\times10^{-3}F_n$ was used; see also Fig. 6). One can expect that several modes with $n \approx n^*$ can contribute to the effective amplitude a_{s0} of the seed signal. The difference in the mode numbers $\Delta n=n^*-n$ causes the angular spread $\Delta\alpha$ around the given scattering angle; this spread should not exceed the admissible value established above, $\Delta\alpha<\cos\alpha/(L_xk_0)\approx\cos\alpha/(2r_0k_0)$. For $|\Delta\alpha|\ll\alpha$ and $|\Delta n|\ll n^*$, one has $\Delta n\approx(k_0r_0/\pi)\cos\alpha\Delta\alpha <\cos^2\alpha/(2\pi)<1$, so that only one capillary mode with $n=n^*$ can contribute to the scattering under the given angle. Therefore, the seed amplitude used for the numerical demonstration of Fig. 4(a) is evaluated as $a_{s0}\approx C_{136}a_0\approx 0.4\times10^{-5}$.

APPENDIX B: DERIVATION OF THE EXACT REFLECTIVE SOLUTION

On omitting k_p^2 in the LHS of Eq. (3b), the Laplace transform (LT) of Eqs. (3) with respect to ξ (LT variable s) and with respect to z (LT variable p) gives the set of ordinary differential equations (ODE) for the Laplace images $\bar{\bar{a}}_{s\pm}(x,p,s;r)$,

$$\left(\frac{\partial}{\partial x}\mp\Omega\right)\bar{\bar{a}}_{s\pm}=\pm K(x), \tag{B1}$$

where $\Omega=(V_z/V_x)(\Gamma_s-p)$, $\Gamma_s=(iG^3/s^2-s)/V_z$, $K(x)=K_1/(sp)+(K_2/s)[1-(2x/L_x-1)^2]$, $K_1=g_1N_0/(iV_x)$, and $K_2=(V_z/V_x)a_{s0}$. The boundary conditions are $\bar{\bar{a}}_{s+}(0,p,s)=r\bar{\bar{a}}_{s-}(0,p,s)$ and $\bar{\bar{a}}_{s-}(L_x,p,s)=r\bar{\bar{a}}_{s+}(L_x,p,s)$. Equations (B1) admit the solution

$$\begin{aligned}\bar{\bar{a}}_{s+}(x,p,s;r)=&-\left(\frac{K_1}{p}+K_2\right)\left[1-\frac{(1-r)e^{\Omega x}}{1-re^{\Omega L_x}}\right]\frac{1}{s\Omega}\\&+\frac{K_2}{(L_x/2)^2}\left\{1+\left[\Omega\left(\frac{L_x}{2}-x\right)-1\right]^2\right\}\frac{1}{s\Omega^3}\\&-\frac{K_2}{(L_x/2)^2}\frac{e^{\Omega x}}{1-re^{\Omega L_x}}\left\{1+\left(\Omega\frac{L_x}{2}-1\right)^2\right.\\&\left.-r\left[1+\left(\Omega\frac{L_x}{2}+1\right)^2\right]\right\}\frac{1}{s\Omega^3},\end{aligned} \tag{B2}$$

where $x_n\equiv x+nL_x$. Lateral symmetry gives $\bar{\bar{a}}_{s-}(x)=\bar{\bar{a}}_{s+}(L_x-x)$. The Laplace transform inversion of Eq. (B2) with respect to p reads

$$\begin{aligned}\overline{a_{s+}}(x,z,s;r)=&-\frac{\tilde{K}_1}{s\Gamma_s}+\left[\tilde{K}_1\frac{e^{\Gamma_s z}}{s\Gamma_s}\right.\\&\left.-\tilde{K}_2\frac{e^{\Gamma_s z}}{s}\frac{(x-\tilde{z})(x-\tilde{z}-L_x)}{(L_x/2)^2}\right]H(x-\tilde{z})\\&+\tilde{K}_1(1-r)\sum_{n=0}^{\infty}r^n\frac{e^{\Gamma_s(V_z/V_x)x_n}}{s\Gamma_s}H(\tilde{z}-x_n)\\&+\sum_{n=1}^{\infty}r^n\left\{\tilde{K}_1\frac{e^{\Gamma_s z}}{s\Gamma_s}\right.\\&\left.-\tilde{K}_2\frac{e^{\Gamma_s z}}{s}\frac{(x_{n-1}-\tilde{z})(x_n-\tilde{z})}{(L_x/2)^2}\right\}[H(\tilde{z}-x_{n-1})\\&-H(\tilde{z}-x_n)],\end{aligned} \tag{B3}$$

where, in accordance with Ref. 14, the expansion $[1-r\exp(\Omega L_x)]^{-1}=\Sigma_{n=0}^{\infty}r^n\exp(n\Omega L_x)$ is used, and $\tilde{z}\equiv(V_x/V_z)z$, $\tilde{K}_{1,2}\equiv(V_x/V_z)K_{1,2}$. Equation (B3) includes Laplace images of the three types: $1/(s\Gamma_s)$, $e^{\Gamma_s y}/(s\Gamma_s)$, and $e^{\Gamma_s y}/s$. Their inversions read

$$\mathcal{L}_s^{-1}\left\{\frac{1}{s\Gamma_s}\right\}=-\frac{V_z}{3}\sum_{j=1}^{3}\frac{e^{c_j\xi}}{c_j}, \tag{B4}$$

where $c_j^3=iG^3$, so that $c_1=-iG$, $c_2=(i+\sqrt{3})G/2$, $c_3=(i-\sqrt{3})G/2$;

$$\mathcal{L}_s^{-1}\left\{\frac{e^{\Gamma_s y}}{s\Gamma_s}\right\}=-\frac{V_z}{3}\sum_{j=1}^{3}\frac{e^{c_j\xi}}{c_j}F_s\left(c_j,\frac{y}{V_z},\xi\right), \tag{B5}$$

which is expressed through the fundamental solutions[21]

$$F_s(\mu,v,\xi)=e^{-\mu v}\sum_{n=0}^{\infty}\frac{(\mu v)^n}{n!\,(2n)!}\gamma[2n+1,\mu(\xi-v)]H(\xi-v), \tag{B6}$$

where $\gamma(m,\theta)=\int_0^\theta e^{-\tau}\tau^{m-1}d\tau=\theta^m\Sigma_{n=0}^{\infty}(-\theta)^n\,[n!(n+m)]$ is the incomplete gamma function of order m of a complex variable θ (Ref. 35); and

$$\mathcal{L}_s^{-1}\{e^{\Gamma_s y}/s\} = \sqrt{\pi} H(\xi - z/V_z)_0\tilde{F}_2(;1,1/2;i\zeta), \tag{B7}$$

expressed through the regularized generalized hypergeometric function[35] of variable $i\zeta = i(G^3/4)(\xi - z/V_z)^2 z/V_z$. Combining expressions (B4), (B5), and (B7) in Eq. (B3) gives the envelope (8a) of an up-going EMW. The amplitude (8b) of the scattering EPW is derived in the similar fashion.

APPENDIX C: ASYMPTOTIC REFLECTIVE SOLUTION

The asymptotic can be found by applying the inversion formula, $\overline{a_{s+}}(x,z,s) = (2\pi i)^{-1}\int_{c-i\infty}^{c+i\infty} e^{px}\bar{\bar{a}}_{s+}(x,p,s)dp$, to the expression (B2). The asymptotic behavior at $z \to \infty$ is determined by the singularities of the integrand at $p=0$, $p=\Gamma_s$, and $p_n = \Gamma_s - \nu + (V_x/V_z)(2\pi n i/L_x)$ with n integer and $\nu = -(V_x/V_z)(\ln r/L_x)$. Expanding $\bar{\bar{A}}_{s+}(x,p,s)$ in the vicinity of the specific points shows that all the singularities at $p = \Gamma_s$ and $p = p_n$ give the contribution $\overline{a_1}(x,z,s) \propto \exp(\Gamma_s z)$. Therefore, $\mathcal{L}_s^{-1}\{\overline{a_1}\} \propto H(\xi - z/V_z)$, and, for a pulse of finite duration, $\xi \leqslant ct_0$, no contribution comes to the asymptotic from these specific points as soon as the distance z from the entrance plane exceeds $V_z ct_0$ [or 0 for $\alpha > \pi/2$]. (Actually, the Laplace image singularities at $p=\Gamma_s$ and $p=p_n$ determine the entrance effect, i.e., the waves produced by the seed at the entrance aperture amplified in the pump field in plasma; these waves inevitably drop behind the laser pulse and their effect therefore vanishes at $z \to \infty$.) The contribution from $p = 0$,

$$\overline{a_{s+}}(x, z \to \infty, s) \sim \frac{1}{s\Gamma_s}\left\{1 - \frac{(1-r)\exp[(V_z/V_x)\Gamma_s x]}{1 - r\exp[(V_z/V_x)\Gamma_s L_x]}\right\}, \tag{C1}$$

thus determines the long-term evolution of instability in plasma, which is dominated by the lateral reflections of scattered EMW. Neither $s = c_j$ (where $\Gamma_s = 0$) nor $s=0$ are the singularities of the image (C1), so contributions to the asymptotic originate from the singular points s_n only, which are the solutions of the equation $\Gamma_{s_n} = \nu_n$ [here, $\nu_n = (V_x/V_z) \times (-\ln r + 2\pi i n)/L_x$] or $s_n^3 + \nu_n V_z s_n^2 - iG^3 = 0$, where n is integer. The fundamental specific point s_0 with the maximum real part is the root of the cubic equation $s^3 + \nu_0 V_z s^2 - iG^3 = 0$ which, for arbitrary ν_0, admits quite a cumbersome explicit expression. We address to the physically interesting limit of low leakage, i.e., $\nu_0 < 3G/V_z$, or $r > \exp(-3GL_x/V_x)$, which means that the scattered EMW gains more energy between two reflections than loses due to leakage through the wall at one reflection. In this case the lateral convection is mostly suppressed. Solution obtained via the perturbation approach reads $s_0 \approx (i+\sqrt{3})G/2 - \nu_0 V_z/3$. Contribution to the asymptotic from that point is of the order of $e^{s_0\xi}$, which grows in time with an increment Re s_0. However, the absolute value of ν_n grows with n, so an evaluation has to be done of the contribution from the points s_n with large n. We again use the perturbation approach with the small parameter $\mu_n = G/(|\nu_n| V_z)$, that is, $n > GL_x/(2\pi V_x)$, and find the solutions $s_n^{(1)} \approx -\nu_n V_z - iG\mu_n^2$, $s_n^{(2,3)} \approx \pm G\sqrt{-(\mathrm{sign}\, n)\mu_n}$. Obviously, Re $s_j \ll G$ for $\mu_n \ll 1$, so that contribution from these points to the asymptotic is negligible compared to that from the points s_n with $n < GL_x/(2\pi V_x)$, which is of the order of $e^{s_0\xi}$. Expanding the image (C1) in the vicinity of $s = s_0$, we arrive at the asymptotic valid for $G\xi \gg 1$,

$$a_{s+}(x,\xi) \sim \frac{V_z}{G}\left(\frac{1-r}{\ln r}\right)\frac{i-\sqrt{3}}{6}\exp\left(s_0\xi - \ln r\frac{x}{L_x}\right), \tag{C2}$$

which represents the unstable solution as a quasi-1D exponentially growing mode.

[1] M. D. Perry and G. Mourou, Science **64**, 917 (1994), and references therein.
[2] N. H. Burnett and G. D. Enright, IEEE J. Quantum Electron. **QE-26**, 1797 (1990).
[3] X. F. Li, A. L'Huillier, M. Ferray, L. A. Lompré, and G. Mainfray, Phys. Rev. A **39**, 5751 (1989).
[4] T. Tajima and J. M. Dawson, Phys. Rev. Lett. **43**, 267 (1979).
[5] N. E. Andreev, L. M. Gorbunov, V. I. Kiranov, A. A. Pogosova, and R. R. Ramazashvili, JETP Lett. **55**, 571 (1992); P. Sprangle, E. Esarey, J. Krall, and C. Joyce, Phys. Rev. Lett. **69**, 2200 (1992); T. Antonsen, Jr. and P. Mora, *ibid.* **69**, 2204 (1992).
[6] E. Esarey, P. Sprangle, J. Krall, and A. Ting, IEEE Trans. Plasma Sci. **PS-24**, 252 (1996).
[7] E. A. J. Marcatili and R. A. Schmeltzer, Bell Syst. Tech. J. **43**, 1783 (1964).
[8] B. Cros, C. Courtois, G. Matthieussent, A. Di Bernardo, D. Batani, N. Andreev, and S. Kuznetsov, Phys. Rev. E **65**, 026405 (2002).
[9] S. Jackel, R. Burris, J. Grun, A. Ting, C. Manka, K. Evans, and J. Kosakowskii, Opt. Lett. **20**, 1086 (1995); M. Borghesi, A. J. Mackinnon, R. Gaillard, O. Willi, and A. A. Offenberger, Phys. Rev. Lett. **80**, 5349 (1998); F. Dorchies, J.-R. Marquès, B. Cros *et al.*, *ibid.* **82**, 4655 (1999).
[10] B. Cros, C. Courtios, G. Malka *et al.*, IEEE Trans. Plasma Sci. **PS-28**, 1071 (2000); C. Courtois, A. Couairon, B. Cros, J.-R. Marquès, and G. Matthieussent, Phys. Plasmas **8**, 3445 (2001); N. E. Andreev, B. Cros, L. M. Gorbunov, G. Matthieussent, P. Mora, and R. R. Ramazashvili, *ibid.* **9**, 3999 (2002).
[11] B. Cros, C. Courtois, J. Godiot *et al.*, Phys. Scr., **T107**, 125 (2004).
[12] N. E. Andreev, Y. Nishida, and N. Yugami, Phys. Rev. E **65**, 056407 (2002).
[13] Y. Kitagawa, Y. Sentoku, S. Akamatsu *et al.*, Phys. Rev. Lett. **92**, 205002 (2004).
[14] C. J. McKinstrie, A. V. Kanaev, and E. J. Turano, Phys. Rev. E **56**, 1032 (1997); E. J. Turano and C. J. McKinstrie, Phys. Plasmas **7**, 5096 (2000).
[15] C. Courtois, Ph.D. thesis, Université Paris XI, Orsay, 2001, in French.
[16] N. E. Andreev, Sov. Phys. JETP **32**, 1141 (1971).
[17] L. M. Gorbunov, Sov. Phys. JETP **40**, 689 (1975); D. W. Forslund, J. M. Kindel, and E. L. Lindman, Phys. Fluids **18**, 1002 (1975).
[18] T. M. Antonsen, Jr. and P. Mora, Phys. Fluids B **5**, 1440 (1993).
[19] C. J. McKinstrie, R. Betti, R. E. Giacone, T. Kolber, and E. J. Turano, Phys. Rev. E **51**, 3752 (1995); C. J. McKinstrie and E. J. Turano, Phys. Plasmas **4**, 3347 (1997).
[20] N. E. Andreev and S. Yu. Kalmykov, IEEE Trans. Plasma Sci. **PS-28**, 1201 (2000).
[21] S. Yu. Kalmykov, Plasma Phys. Rep. **26**, 938 (2000).
[22] Ph. Mounaix, D. Pesme, W. Rozmus, and M. Casanova, Phys. Fluids B **5**, 3304 (1993); C. Rousseaux, G. Malka, J. L. Miquel, F. Amiranoff, S. D. Baton, and Ph. Mounaix, Phys. Rev. Lett. **74**, 4655 (1995).
[23] S. V. Bulanov, F. Pegoraro, and A. M. Pukhov, Phys. Rev. Lett. **74**, 710 (1995); C. D. Decker, W. B. Mori, K.-C. Tzeng, and T. Katsouleas, Phys. Plasmas **3**, 2047 (1996).
[24] K.-C. Tzeng and W. B. Mori, Phys. Rev. Lett. **81**, 104 (1998).
[25] S. C. Wilks, W. L. Kruer, E. A. Williams, P. Amendt, and D. C. Eder, Phys. Plasmas **2**, 274 (1995); C. I. Moore, A. Ting, K. Krushelnick *et al.*, Phys. Rev. Lett. **79**, 3909 (1997); E. Esarey, B. Hafizi, R. Hubbard, and P. Sprangle, *ibid.* **80**, 5552 (1998); M. Fomitskyi, C. Chiu, M. Downer, and F. Grigsby, Phys. Plasmas **12**, 023103 (2005).
[26] A. S. Sakharov and V. I. Kirsanov, Phys. Rev. E **49**, 3274 (1994).
[27] D. F. Gordon, B. Hafizi, P. Sprangle, R. F. Hubbard, J. R. Peñano, and W. B. Mori, Phys. Rev. E **64**, 046404 (2001).
[28] D. L. Bobroff and H. A. Haus, J. Appl. Phys. **38**, 390 (1967).
[29] C. B. Darrow, C. Coverdale, M. D. Perry, W. B. Mori, C. Clayton,

K. Marsh, and C. Joshi, Phys. Rev. Lett. **69**, 442 (1992); A. Ting, K. Krushelnick, H. R. Burris, A. Fisher, C. Manka, and C. I. Moore, Opt. Lett. **21**, 1096 (1996); K. Krushelnick, C. I. Moore, A. Ting, and H. R. Burris, Phys. Rev. E **58**, 4030 (1998).
[30]Ph. Mounaix and D. Pesme, Phys. Plasmas **1**, 2579 (1994).
[31]P. Mora and T. M. Antonsen, Jr., Phys. Plasmas **4**, 217 (1997).
[32]N. E. Andreev (private communication).
[33]W. B. Mori, C. D. Decker, D. E. Hinkel, and T. Katsouleas, Phys. Rev. Lett. **72**, 1482 (1994); C. J. McKinstrie and E. J. Turano, Phys. Plasmas **3**, 4683 (1996).
[34]N. E. Andreev, V. I. Kirsanov, L. M. Gorbunov, and A. S. Sakharov, IEEE Trans. Plasma Sci. **PS-24**, 363 (1996); N. E. Andreev, L. M. Gorbunov, V. I. Kirsanov, A. A. Pogosova, and A. S. Sakharov, Plasma Phys. Rep. **22**, 379 (1996).
[35]E. W. Weisstein, *Incomplete Gamma Function*, http://functions.wolfram.com/06.06.02.0001.01; *Regularized Generalized Hypergeometric Function*, http://functions.wolfram.com/07.32.06.0035.01; From MATH WORLD—A Wolfram Web Resource (Wolfram Research, Inc., Champaign, Illinois, 1999–2005)
[36]S. Yu. Kalmykov, Ph.D. thesis, Associated Institute for High Temperatures, Russian Academy of Sciences, Moscow, 2001, in Russian.
[37]A. I. Akhiezer, I. A. Akhiezer, R. V. Polovin, A. G. Sitenko, and K. N. Stepanov, *Plasma Electrodynamics*, Nonlinear Theory and Fluctuations, Vol 2 (Pergamon, Oxford, 1975), p. 132.
[38]A. S. Sakharov, Plasma Phys. Rep. **26**, 657 (2000).